World Electric Vehicle Journal

MDPI

Article

Research on the Electromagnetic-Heat-Flow Coupled Modeling and Analysis for In-Wheel Motor

Haojie Xue, Di Tan *, Shuaishuai Liu, Meng Yuan and Chunming Zhao

School of Transportation and Vehicle Engineering, Shandong University of Technology, 12 Zhangzhou Road, Zhangdian, Zibo 255049, China; clgcxhj@163.com (H.X.); 15684139983@163.com (S.L.); 13295351580@163.com (M.Y.); z1395524640@163.com (C.Z.)

* Correspondence: tandi@sdut.edu.cn

Received: 14 February 2020; Accepted: 18 March 2020; Published: 25 March 2020

Abstract: In this paper, a 15 KW in-wheel motor (IWM) is taken as the research object, and the coupling factors among the electromagnetic field, temperature field and flow field are analyzed, and the strong and weak coupling factors between the three fields are clarified, and by identifying the strong and weak coupling factors between the three fields, a three-field coupling analysis model for IWM with appropriate complexity is established, and the validity of the model is verified. In a certain driving condition, the electromagnetic field, temperature field and flow field characteristics of IWM are analyzed with the multi-field coupling model. The result shows that, after the IWM runs 8440 s under driving conditions, in this paper, the IWM electromagnetic torque of the rated working condition is 134.2 Nm, and IWM the electromagnetic torque of the peak working condition is 451.36 Nm, and the power requirement of the motor can be guaranteed. The highest temperature of the IWM is 150 °C, which does not exceed the insulation grade requirements of the motor (155 °C), the highest temperature of the permanent magnet (PM) is 65.6 °C, and it does not exceed the highest operating temperature of the PM, and ensures the accurate calculation of components loss and the temperature of the motor. It can be found, through research, that the electromagnetic torque difference between unidirectional coupling and bidirectional coupling is 3.2%, the maximum temperature difference is 7.98% in the three-field coupling analysis of IWM under rated working conditions. Therefore, it is necessary to consider the influence of coupling factors on the properties of motor materials when analyzing the electromagnetic field, temperature field and flow field of IWM; it also provides some reference value for the simulation analysis of IWM in the future.

Keywords: in-wheel motor; three-field coupling; coupling factors; running condition

1. Introduction

As an important part of the electric vehicle drive system, it is necessary to accurately analyze the electromagnetic characteristics, temperature characteristics and flow field characteristics of the in-wheel motor (IWM). The core loss, copper loss and permanent magnet (PM) eddy current loss of IWM are calculated by an electromagnetic field, the loss is used as a heat source to calculate the highest temperature of each component, and the simulation analysis of the flow field is carried out to make the IWM dissipate heat. The change of temperature affects the material properties of the components of the IWM electromagnetic field, and then the loss of each component of the motor can be influenced, and the change of loss also affects the temperature. At the same time, temperature also affects the material properties of the fluid in the flow field, the change of fluid properties having an effect on temperature. The alternating magnetic field generated by the electromagnetic field also has an effect on the fluid properties; the change of fluid property affects the flux density of the motor electromagnetic

field, and then affects the loss of the motor. Therefore, in the process of motor operation, the various physical fields interact and influence each other.

At present, there are many literatures about the electromagnetic field, flow field and heat field of the IWM at home and abroad, and the achieved fruitful research results. Shanlin Jiang took a high-speed PM synchronous motor as the research object, in the electromagnetic-heat coupling simulation; the relationship between motor loss, PM residual flux density and temperature was considered, and the results were compared with those without considering the effect of temperature. It was concluded that temperature had a great influence on motor performance and loss [1]. Driesen U et al. took a PM synchronous electrical vehicle motor as the research object, In the finite element simulation, the temperature dependence of the PM and the conductive material of the motor was considered, the electromagnetic-heat coupling analysis was realized and the loss of the motor was calculated in detail, and in order to avoid the numerical problems of the electromagnetic field and temperature field, the losses were calculated on different time scales, which makes the results more accurate [2]. Alberti L et al. took induction motor as the research object, and an electromagnetic-heat coupling analysis method was proposed. Firstly, the finite element model was established to analyze the electromagnetic field, and determined the parameters of the equivalent circuit. Then, a thermal mesh model was established, the equivalent circuit was coupled with the thermal grid model, and the temperatures of the different parts of the motor were calculated; the convergence rate of this method was very fast, and also had better calculation accuracy [3]. S. Mezani et al. took an induction motor and established a mathematical model of electromagnetic-thermal coupling; the equivalent thermal mesh method is used in the temperature field, and the finite element method was used in the electromagnetic field; the validity and accuracy of the results were verified by experiments [4]. Qi Zhang et al. took a 48-slot 8-pole PM motor for vehicles, and established a three-dimensional model, studied the flow field and thermal field of the motor, and a temperature rise test was carried out to verify the validity and accuracy of the simulation analysis method, however, the effect of temperature on the fluid properties was not considered [5]. Xiaoyuan Wang et al. took a 8.5 KW external rotor PM synchronous IWM as the research object, and establishing a two-dimensional finite element model, the influence of temperature on the material properties of the motor was considered, and the heating of the motor and the temperature field distribution in the motor were studied [6]. V. Hatziathanassiou et al. took an asynchronous motor as the research object, an equivalent circuit was used for the electromagnetic field and the finite element method was used for the temperature field; the coupled calculation of the temperature field and electromagnetic field of the motor was carried out under transient conditions. At each time step, the effect of temperature on the winding resistance and current was considered, and the temperature distribution of the motor was obtained [7]. Nannan Zhao et al. took the brushless direct-current (DC) motor as the research object, and the electromagnetic-heat coupling method was used to calculate the loss and temperature field of the motor. Firstly, the motor loss was calculated by the finite element simulation of the electromagnetic field, the loss was loaded into the temperature field as a heat source and the temperature distribution of the motor was calculated. Then, the influence of temperature on the electromagnetic field was considered, and the electromagnetic field was recalculated. This approach was compared with unidirectional coupling, and the accuracy of the calculation had improved, however, the influence of temperature on the electromagnetic field was not taken into account in every iteration of the calculation [8]. Nansha Gao et al. took a 200 KW, 60,000 rpm high-speed PM motor as the research object, and established a two-dimensional finite element model; the analytical method and finite element method were used to calculate the various losses of the motor. The temperature distribution of each part of the motor and the highest temperature of the motor were obtained [9]. Minghui Zhang et al. took the PM brushless DC motor as the research object, a two-dimensional model was built, the electromagnetic-heat coupling simulation of the motor was carried out, and the relationship between the conductive material and the temperature of the motor was considered; the relationship between the PM and temperature can also be considered, but it was a two-dimensional model, and the axial temperature distribution of the motor was not considered [10].

Xiaowei Wang et al. took the brushless DC motor as the research object, and the electromagnetic field simulation results, rotor core and winding loss as heat source, imported into the temperature field. The temperature distribution of the motor was calculated, but this coupling was simply unidirectional coupling, and there was a certain difference between the simulation value and the experimental value; the simulation results were inaccurate [11]. Lixiu Zhang et al. took the machine motor spindle as the research object, and the prediction model of spindle temperature field for high speed motor under different working conditions was established, and the influence of the cooling system on the heat transfer coefficient of the motor spindle was considered [12].

Jae-Bum Park et al. took a 3 KW permanent magnet synchronous motor as the research object, and establishing a three-dimensional finite element model, the coupling analysis of the electromagnetic field and temperature field of the motor was carried out, and the influence of temperature on the material properties of the electromagnetic field was considered, with the copper loss and iron loss of the motor and the temperature distribution of the motor being calculated [13]. Yannis L. Karnavas et al. took a permanent magnet synchronous motor as the research object, and established a three-dimensional finite element model; the temperature distribution of the motor was determined by a finite element simulation under different working conditions, and the optimum cooling effect was determined by changing the inlet temperature and flow rate of the coolant [14]. My-Ismail Lamghari-Jamal et al. presented a magneto-thermal model of a high-speed synchronous reluctance machine, the fundamental principles of magnetism and heat were applied, and they established a three-dimensional and two-dimensional finite element model, with the motor convection exchange coefficient being considered [15]. Li Junqing et al. presented a coupling mathematical model of the electromagnetic and temperature field and calculated them using the finite element method, and the influence of temperature on the material properties of the motor was considered [16]. Ding Shuye et al. took a 1.5 MW doubly-fed wind generator as the research object, and established a three-dimensional finite element model, the fluid field and temperature field in the generator coupled by the finite volume element method, and the velocity and flow distribution of the cooling air in the flow area were obtained [17]. It can be seen from the above references, at present, that in the simulation analysis of IWM at home and abroad, coupling factors are not considered comprehensively, and moreover, it is not based on a driving condition analysis, which makes the simulation results inaccurate.

In summary, many experts, both foreign and domestic, have done a lot of research on the electromagnetic field, temperature field and flow field of IWM, and have obtained beneficial results. However, in the current study, most of them are for the local two-field coupling analysis, and in two-field studies, the coupling factor is not very comprehensive, so the calculation accuracy has some deviation, and most of them are based on a single working condition. In this paper, a 15-KW (IWM) is taken as the research object, the coupling factors among electromagnetic field; the temperature field and flow field are fully analyzed, and strong coupling factors are considered and weak coupling factors are ignored. A three-field coupling model is thus established, the correctness of the model is verified, and under the condition of acceleration, uniform, climbing and deceleration conditions, a coupling analysis of the multi-physical fields is carried out for IWM.

2. Structure of IWM

2.1. Basic Structure of IWM

The basic structure of the IWM is shown in Figure 1. The IWM has an inner rotor and an outer stator, and the rotor connects the rim to drive the vehicle directly, and the motor cooling structure is a spiral cooling structure [18].

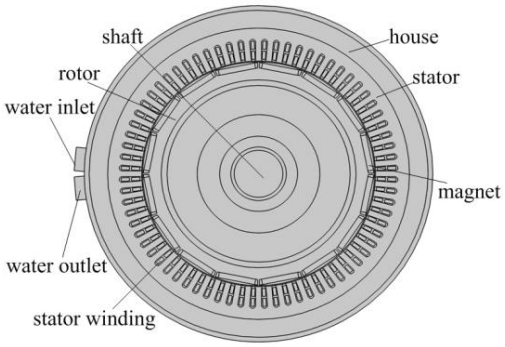

Figure 1. The structure of the in-wheel motor (IWM).

2.2. Basic Parameters of IWM

The specific structural dimensions and electromagnetic parameters of the IWM are shown in Tables 1 and 2.

Table 1. Structure parameters of IWM.

Name	Numerical Value	Name	Numerical Value
Stator outer diameter	310 mm	Rotor inner diameter	200 mm
Stator inner diameter	240 mm	Air gap length	0.9 mm
Stator length	69 mm	Rotor length	71 mm
Diameter of inlet and outlet	15 mm	Rib width	4 mm
Channel cross section	232 mm^2	Channel height	10 mm

Table 2. Technical parameters of IWM.

Name	Numerical Value	Name	Numerical Value
Rated power	15 KW	Speak speed	1100 rpm
Peak power	54 KW	Rated speed	1000 rpm

3. Analysis of Electromagnetic-Heat-Flow Coupling Factors

The influence factors of the electromagnetic field and temperature field are mainly reflected in the conversion of motor loss into heat energy, the temperature of the motor is increased, and the change of temperature affects the material properties of motor, such as conductivity, residual flux density, etc. The influence factors of the temperature field and flow field are mainly reflected, in that fluid properties change with temperature, such as density, thermal conductivity, dynamic viscosity, specific heat capacity, etc., and the change of fluid properties also affects the temperature, thus, the electromagnetic field of the motor material properties can be affected. The influence factors of the electromagnetic field and flow field are mainly reflected in the alternating magnetic generated by the electromagnetic field, which has an effect on the fluid properties, and the change of fluid property also affects the flux density of the motor electromagnetic field, and then affects the loss of the motor. The electromagnetic-heat field and flow-heat field are direct influences, and the electromagnetic-flow field is an indirect influence. The specific schematic diagram is shown in Figure 2.

3.1. Analysis of the Coupling Factors of Electromagnetic Field and Temperature Field

3.1.1. Influence Factors of Electromagnetic Field on Temperature Field

The influence factor of the electromagnetic field on the temperature field is the loss, that is, the heat generation rate in the temperature field. The calculation formula is as follows [19]:

$$q = P_{loss}/V \quad (1)$$

where q is the heat generation per unit volume, W/m^3; P_{loss} is the loss of each part of the IWM, W; V is the effective volume of each part of the IWM, m^3.

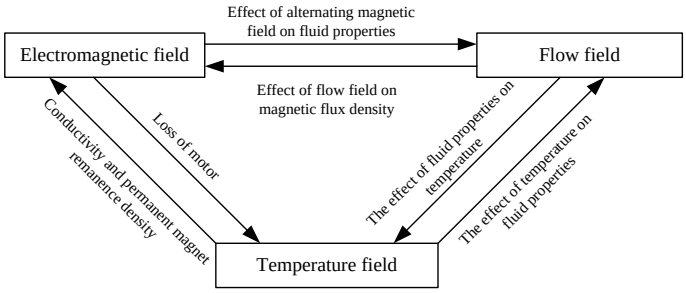

Figure 2. Schematic diagram of three-field coupling relationship.

(1) Core Loss

Core loss can be classified as: hysteresis loss, eddy current loss and additional loss. The core loss calculation formula is as follows [20]:

$$P_{Fe} = P_h + P_c + P_e \tag{2}$$

$$P_h = K_h f B_m^{\alpha} \tag{3}$$

$$P_c = K_c f^2 B_m^2 \tag{4}$$

$$P_e = K_e f^{1.5} B_m^{1.5} \tag{5}$$

$$K_c = \pi^2 \sigma d^2 / 6 \tag{6}$$

where, P_{Fe} is the core loss, W/m^3; P_h is the hysteresis loss of iron core, W/m^3; P_c is the eddy current loss of iron core, W/m^3; K_h and K_c are the coefficients of the hysteresis loss and eddy current loss, W/kg; P_e is the additional core loss, W/m^3; K_e is the coefficient of the additional core loss, W/kg, Through simulation calculation, the additional iron loss is 7.49×10^{-13} W, the value of the additional core loss is so small that it is almost negligible; B_m is the amplitude of the flux density, T; f is the magnetic field frequency, Hz; α is the empirical coefficient, and the general value is 2; σ is the conductivity, S/m; d is the thickness of silicon steel sheet, mm.

(2) Eddy Current Loss of the PM

The periodic change of the magnetic flux density of the motor also causes the eddy current loss of the PM. The eddy current loss of PM can be calculated by the following formula [21]:

$$P = \int \frac{J^2}{2\sigma} dv \tag{7}$$

where P is the PM eddy current loss, W; J is the vortex density of the PM, A/m^2; and σ is the conductivity of the PM, S/m.

(3) Copper Loss

The winding copper loss is the main heat source of the IWM. It is mainly due to the electrical winding, which is related to the winding current and the winding resistance. According to Joule–Lenz's law. The winding loss calculation formula is as follows [22]:

$$P_{cu} = mI^2R \tag{8}$$

where P_{cu} is the winding copper loss, W; m is the phase number of the IWM, take 3; I is the winding current, A; R is the winding resistance at the reference operating temperature, Ω.

3.1.2. Influence of Temperature Field on Electromagnetic Field

The influence of temperature field on electromagnetic field is mainly manifested in the change of material properties of the motor with temperature.

(1) Influence of Temperature on the Conductivity of Materials

The resistance of the copper can be calculated by the following formula:

$$R = \rho \frac{L}{S} \tag{9}$$

where R is the resistance, Ω; ρ is the resistivity, Ω·m; L is the length of the conductor, cm; S is the cross-sectional area of the conductor, mm^2.

The relationship between resistivity and temperature can be calculated from the following formula [23]:

$$\rho = \rho_{20}[1 + (t - t_{20})] \tag{10}$$

where ρ is the temperature coefficient of resistance; ρ_{20} is the resistivity at a temperature of 20 °C; t_{20} is the 20 °C.

The temperature change of IWM has a great influence on the conductivity of the stator core, rotor core, PM and the winding of the motor. Therefore, the change of material properties caused by the temperature will lead to the change of motor loss. The conductivity of each component of the motor changes with temperature, as shown in Figure 3.

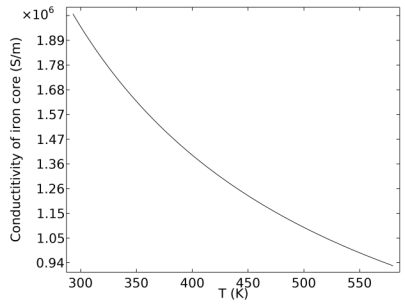

(**a**) The iron core conductivity curve changes with temperature

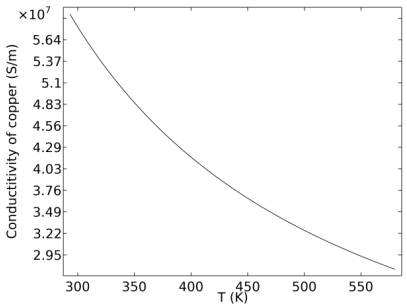

(**b**) The copper conductivity curve changes with temperature

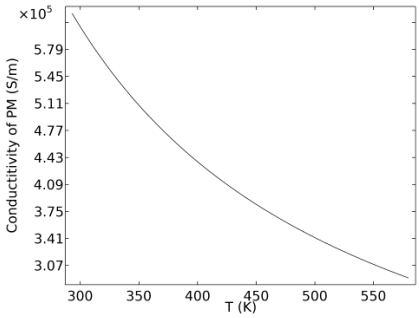

(**c**) The PM conductivity curve changes with temperature

Figure 3. The conductivity curve changes with temperature.

(2) Influence of Temperature on Residual Flux Density of PM

As the permanent magnetic material with the highest magnetic performance, NdFeB PM material has a higher temperature coefficient, and the thermal stability of magnetic properties is poor; the temperature coefficient of B_r is $-0.12\%\ K^{-1}$ [24]:

$$B_r = B_{r20}[1 + \alpha_{Br}(t - 20)] \tag{11}$$

where B_{r20} is the residual flux density at 20 °C, 1.158 T; α_{Br} is the temperature coefficient of NdFeB PM.

The residual flux density of the PM changes with temperature, as shown in Figure 4.

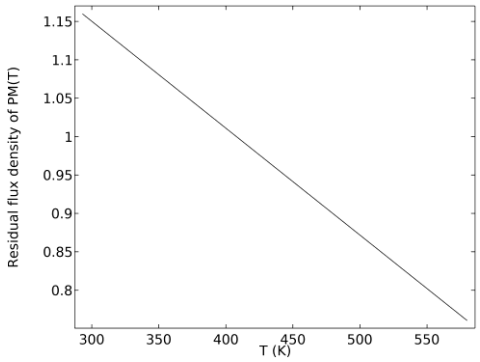

Figure 4. The PM residual flux density curve changes with temperature.

3.2. Analysis of the Coupling Factors of Temperature Field and Flow Field

The effect of temperature on the flow field is mainly reflected in the influence on the fluid properties. The fluid is water in this paper, not ferromagnetic fluid, and is considered a compressible fluid. Therefore, water density, thermal conductivity, dynamic viscosity, and specific heat capacity all change with temperature.

3.2.1. Influence of Temperature on Thermal Conductivity of Fluid

The thermal conductivity is numerically equal to the heat flux conducted per unit area, perpendicular to the heat flux density under a unit temperature gradient. The calculation formula is as follows [25]:

$$\lambda = \frac{q}{-gradt} \tag{12}$$

where λ is the thermal conductivity, $W/(m{\cdot}K)$; q is the heat flux density in this direction, W/m^2; $gradt$ is the temperature gradient in this direction, K/m; the negative sign indicates that the heat transfer points to the direction of the temperature decrease, contrary to the direction of the temperature gradient.

The thermal conductivity of the water changes with temperature, as shown in Figure 5.

As you can see from Figure 5, as the temperature increases, the thermal conductivity first increases and then decreases, the heat generated by the stator core and stator windings is transmitted to the cooling water, and the heat of the cooling water conduction also first increases and then decreases, therefore, the change of thermal conductivity will have a great influence on the overall temperature of the motor.

3.2.2. Influence of Temperature on the Specific Heat Capacity of Fluid

The specific heat capacity means that under constant pressure conditions, when the substance absorbs or releases heat per unit mass and causes the temperature to rise or decrease, the amount

of heat absorbed for every 1K increases in temperature, or the amount of heat released for every 1K decreases in temperature. The calculation formula is as follows [25]:

$$C_p = \frac{\delta Q_p}{dT} \tag{13}$$

where C_p is the specific heat capacity, $J/(Kg{\cdot}K)$; δQ_p indicates the amount of heat absorbed during a certain period of time, dT indicates how much the temperature increases or decreases during a certain period of time.

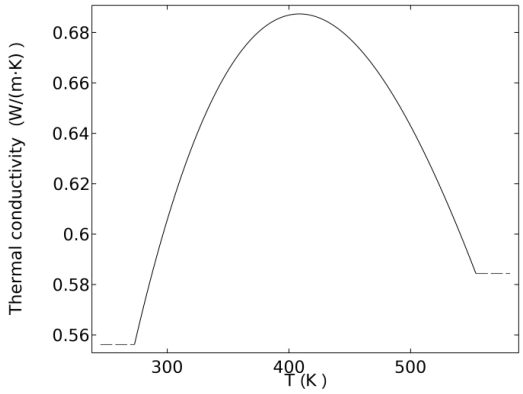

Figure 5. The thermal conductivity of the water changes with temperature.

The specific heat capacity of the water changes with temperature, as shown in Figure 6.

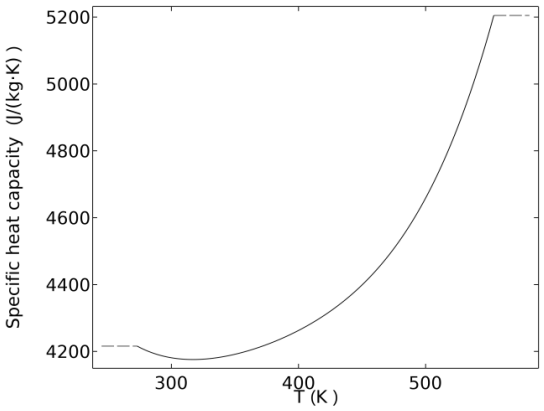

Figure 6. The specific heat capacity of the water changes with temperature.

As can be seen from Figure 6, as the temperature increases, the specific heat capacity first decreases and then increases. This indicates that the heat absorbed by cooling water first decreases and then increases, for every 1K increase in temperature. It also affects the temperature of the motor.

3.2.3. Influence of Temperature on the Dynamic Viscosity of Fluid

The dynamic viscosity is numerically equal to two plates, with an area of 1 m^2 and a distance of 1 m, when relative motion is at a speed of 1 m/s, and internal friction is caused by the interaction of fluids. The calculation formula is as follows [26]:

$$\mu = \frac{0.001779}{1 + 0.03368t + 0.000221t^2} \tag{14}$$

where μ is the dynamic viscosity, $Pa{\cdot}s$; t is the temperature, K.

The dynamic viscosity of the water changes with temperature, as shown in Figure 7.

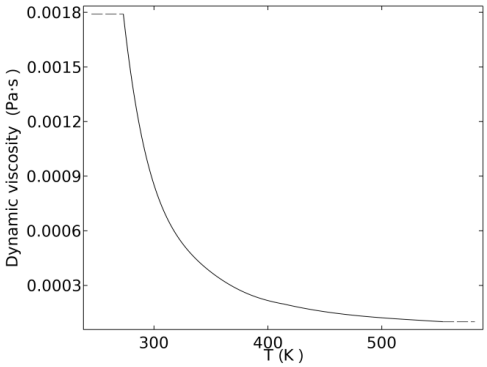

Figure 7. The dynamic viscosity of the water changes with temperature.

As you can see from Figure 7, as the temperature increases, the dynamic viscosity gradually decreases, the friction between fluids gradually decreases, the flow rate gradually increases, and the temperature of the motor gradually decreases.

3.2.4. Influence of Temperature on the Density of Fluid

Density is a measure of the mass within a particular volume. The density is equal to the mass of the object divided by the volume. The calculation formula is as follows:

$$\rho = \frac{m}{v} \tag{15}$$

where ρ is the density, kg/m^3; m is the mass, kg; v is the volume, m^3.

The density of the water changes with temperature, as shown in Figure 8.

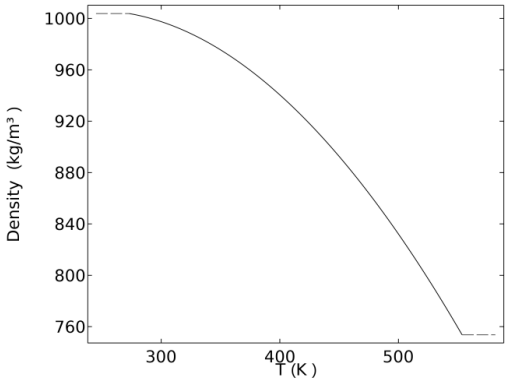

Figure 8. The density of the water changes with temperature.

As you can see from Figure 8, as the temperature increases, the density gradually decreases under the premise of a certain volume of fluid, the mass of fluid decreases gradually, the flow rate gradually increases, and the temperature of the motor gradually decreases.

As you can see from Figures 3–8, the motor is in the process of cooling, and under the influence of fluid properties, the motor temperature changes; they affect and change each other.

3.3. Analysis of the Coupling Factors of Electromagnetic Field and Flow Field

By a finite element simulation analysis of the electromagnetic-flow field of in-wheel motor (IWM), the simulation results of the electromagnetic-flow field coupling are obtained. Compared with the simulation results of the single field electromagnetic field and flow field, it is verified that the mutual

coupling factors between electromagnetic and flow coupling have little influence on the coupling simulation results. The specific comparison results are shown in Figure 9.

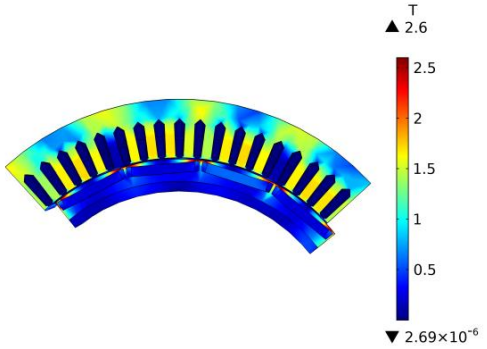

(**a**) Bidirectional coupling magnetic flux density diagram.

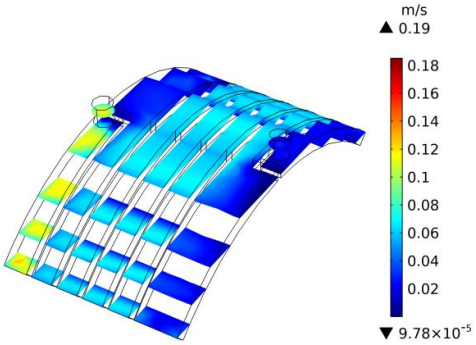

(**b**) Bidirectional coupling velocity diagram.

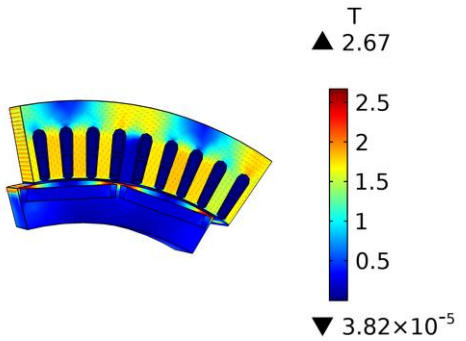

(**c**) Unidirectional coupling magnetic flux density diagram.

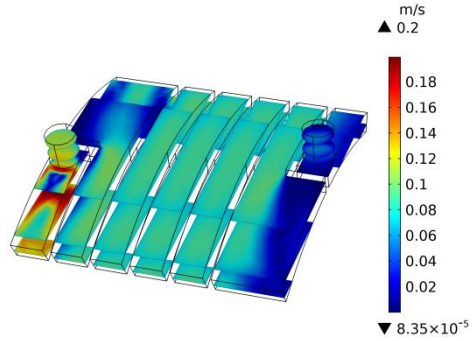

(**d**) Unidirectional coupling velocity diagram.

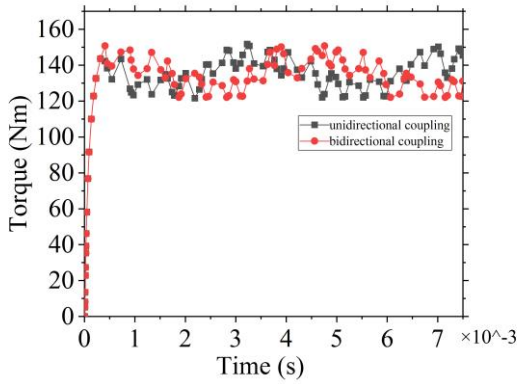

(**e**) Unidirectional coupling and bidirectional coupling torque change curves.

Figure 9. Unidirectional coupling and bidirectional coupling simulation results.

As can be seen from Figure 9, the maximum electromagnetic-flow coupling flux density of IWM is 2.6 T, which appears on the rotor core near the permanent magnet section. The average torque is 139.36 Nm. The maximum flow velocity is 0.19 m/s and occurs on the inlet water side. The maximum magnetic flux density calculated by the unidirectional coupling electromagnetic simulation is 2.67 T, and it also appears on the rotor core near the permanent magnet section; the average torque is 139.02 Nm, and the maximum flow velocity is 0.2 m/s, and it also appears on the inlet side.

Through the above analysis, the maximum value of the flux density and the distribution of flux density obtained by bidirectional coupling and unidirectional coupling of the electromagnetic-flow field are not significantly different, the maximum flux density difference is 2.6%, and the average torque difference is 0.24%, and it is almost negligible. The maximum flow velocity and flow velocity distribution of unidirectional and bidirectional coupled fluid have little difference; the maximum flow velocity difference is 5%. Therefore, the coupling factors between the electromagnetic field and flow field have little influence on each other.

In summary, the temperature affects the conductivity of the materials in the electromagnetic field and the residual flux density of the PM, as well as the thermal conductivity, density, specific heat capacity and dynamic viscosity of the fluid in the flow field. Meanwhile, the change of the material and fluid property of the electromagnetic field will affect the temperature. Therefore, the coupling relationship between electromagnetic field and temperature field is a strong coupling and the coupling relationship between flow field and temperature field is also a strong coupling. The alternating electromagnetic field generated by the electromagnetic field has little effect on the fluid properties, and they are a weak coupling. Therefore, the schematic diagram of the coupling relationship between the three fields can be changed as shown in Figure 10.

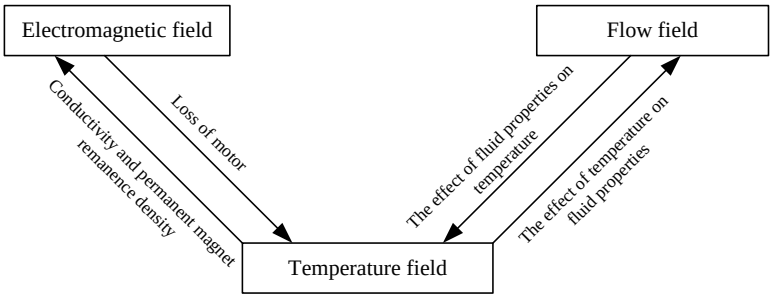

Figure 10. Schematic diagram of strong coupling relationship.

4. The Establishment of Electromagnetic-Fluid-Thermal Coupling Model for IWM and Model Validity Verification

4.1. The Establishment of the Finite Element Model of IWM

The finite element model is established according to the structure and parameters of IWM. The structure of the IWM is shown in Figure 11.

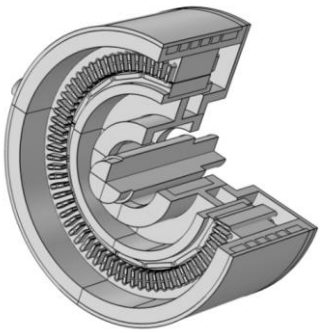

Figure 11. Schematic diagram of three-field coupling model.

4.2. Determination of Boundary Conditions and Material Properties of IWM

4.2.1. Determination of Material Properties of IWM

Silicon steel sheet material DW465-50 is used as the core material of the motor stator and rotor, and the winding material is copper; the rotor bracket, casing and shaft material are steel; the PM material is NdFeB (material grades: N33UH). The material properties of each part of IWM can be obtained as shown in Table 3.

Table 3. Material properties of components.

Component	Material	Thermal Conductivity ($W/(m{\cdot}K)$)	Density (kg/m^3)	Specific Heat Capacity ($J/(Kg{\cdot}K)$)
Stator and rotor core	DW465-50	40/40/0.95	7700	426
Winding	copper	379	8900	390
PM	NdFeB	6.16	7800	460
Insulation layer	Insulation material	0.3	1300	1340
Housing	45 steel	50.2	7850	480
Air	Air	0.0267	1.29	1000

4.2.2. Determination of Boundary Conditions of IWM

(1) With the convection heat transfer generated on the outer surface of the casing circumferentially and on both sides of the casing axially, it is necessary to calculate the surface heat dissipation coefficient. The calculation formula is as follows [27]:

$$\alpha = \alpha_0(1 + 0.5\sqrt{v})^3\sqrt{\frac{\theta}{25}} \tag{16}$$

where α_0 is the heat transfer coefficient of the object surface under static air, the value is 14; v is the air flow velocity on the outer surface, m/s; θ is the air temperature on the outer surface, the value is 20. Through calculation, the heat dissipation coefficient of the outer surface of the casing circumferentially is 41.9 $W/\left(m^2{\cdot}K\right)$ and that of the two side surface of the casing axially is 37.2 $W/\left(m^2{\cdot}K\right)$.

(2) The core of stator and rotor is bounded by Ampere's law, and the air part of the stator part also needs to be set to Ampere's law, while the other regions are bounded by Gauss' law. Then, the current of stator winding is set up.

(3) When determining the boundary conditions of the fluid inlet and outlet, it is assumed that the temperature difference between the inlet and outlet is 20 °C; the inlet temperature and ambient temperature are both set to 20 °C, and it is assumed that the total loss will be taken away by the cooling water, and the inlet flow can be calculated by the following formula [28]:

$$m = \frac{P_{loss}}{C_p(T_{out} - T_{in})} \tag{17}$$

where m is the inlet flow, kg/s; P_{loss} is the total loss of the IWM, W; C_p is the specific heat capacity of cooling water, $J/(kg/K)$, and T_{out}, T_{in} is the outlet and inlet temperature.

The inlet velocity of the water is 0.11 m/s and 0.76 m/s under the rated and peak working condition.

(4) The flow state of the cooling liquid will directly affect the distribution of the temperature field of the motor. Therefore, it is necessary to determine that its flow state in the pipe is laminar flow or turbulence flow. The Reynolds number of cooling water is calculated by [29]:

$$R_e = \frac{\rho u d}{\mu} \tag{18}$$

where R_e is the Reynolds number, ρ is the density of cooling water, kg/m^3; u is the flow rate of cooling water, m/s; d is the equivalent diameter, m; and μ is the dynamic viscosity of cooling water, $Pa{\cdot}s$.

When $R_e < 2300$, the flow state is laminar flow, when $2300 < R_e < 4000$, this is the transition state, when $R_e > 4000$, the flow state is turbulent flow.

It can be known from the calculation that the Reynolds number is greater than 4000 and its flow state is turbulent flow.

4.3. Grid Division of IWM

With the grid division of IWM, the fluid part needs to use the boundary layer grid, and the dynamic mesh is set for the rotating part of the motor. In the two sides of the air gap, the one side in the rotating region needs to be more refined than the one in the fixed region. At the same time, for coils with relatively high grid requirements, the degree of meshing is refined.

4.4. Model Validity Verification

This paper uses the analytical method to verify the correctness of the three-field coupling model. With three-field coupling simulation analysis based on rated condition, the analytical method is based on the copper loss calculation formula (6), the theoretical value of copper loss is 642.33 W, according to the torque formula $T = 9550P/n$, the theoretical value of torque is 143.25 Nm; the copper loss and torque obtained by software simulation is as shown in Figure 12, and the simulation results are compared with the theoretical values.

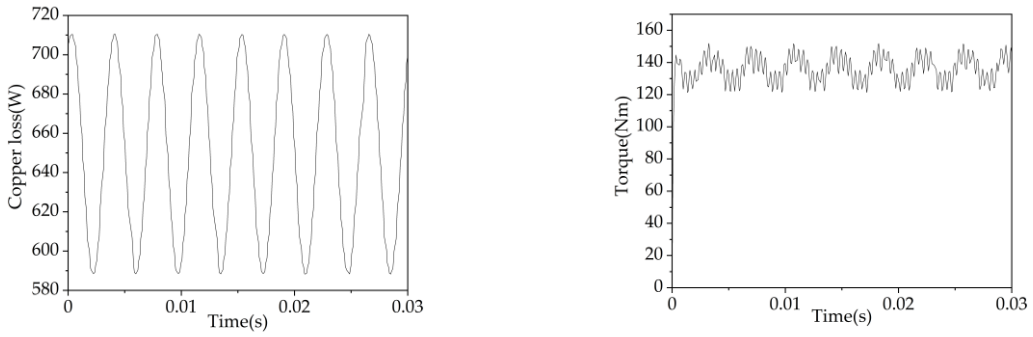

(**a**) Copper loss (**b**) Torque

Figure 12. Copper loss and torque of the rated working condition of IWM.

By comparing the finite element simulation results with the theoretical values calculated by the formula, the conclusion is drawn. Figure 12a shows that the average copper loss is 645.36 W, it differs from the formula calculation result by 3.03 W, and the error is 0.56%; Figure 12b shows that the average torque is 138.6 Nm, it differs from the formula calculation result by 4.65 Nm and the error is 3.2%, the error didn't exceed 5%, and it can be considered that the three-coupling model is correct.

4.5. Three-Field Coupling Calculation Method

In the process of the solution, the multi-physical field interface is set up, and the multi-physical field interface is divided into three parts. The first part is non-isothermal flow, which is set to couple turbulence and heat transfer modules; The second part is temperature coupling, which is set to couple heat transfer and turbulence modules; The third part is the electromagnetic-heat coupling, which is set to couple rotating mechanical electromagnetic and heat transfer modules. At the time of the solution, a coupling analysis is carried out in each iteration.

5. Analysis of Electromagnetic-Heat-Flow Coupling, Based on Working Conditions

5.1. Comparison and Analysis of the Simulation Results of Unidirectional Coupling and Bidirectional Coupling

Under rated conditions and the analysis of electromagnetic-heat-flow coupling simulation, the coupling factors between the three fields is considered; the flow-heat simulation takes the loss of the electromagnetic field as the heat source, and loads into the flow-heat field, the coupling factors between the electromagnetic field and temperature field are not considered, the coupling factors between the flow field and the temperature field are considered, and the motor temperature results are compared and analyzed, as shown in Figure 13.

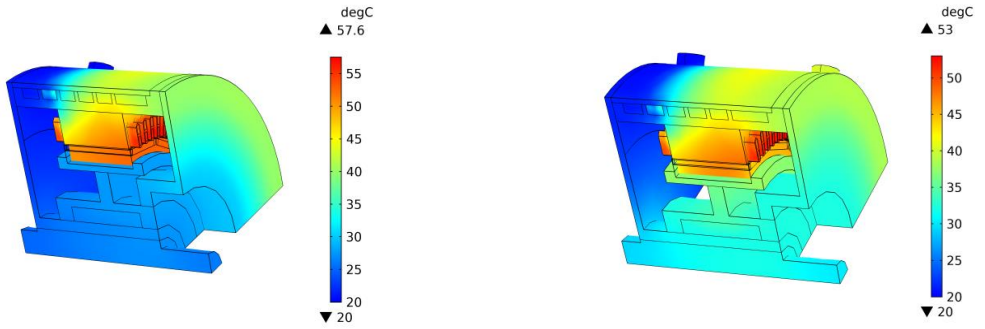

(**a**) Simulation results of electromagnetic-thermal-current three-field coupling

(**b**) Flow-heat simulation results

Figure 13. In-wheel motor temperature diagram.

As you can see from Figure 13, the maximum temperature of the three-field coupling simulation under the rated working condition occurs at the winding part, the maximum temperature is 57.6 °C; the maximum temperature of the flow-heat simulation also appears in the winding part. The maximum temperature is 53 °C. The maximum temperature of each part of the IWM is shown in Table 4.

Table 4. Comparison of IWM maximum temperature.

	Maximum Temperature (°C)			
	Stator Core	**Rotor Core**	**Winding**	**PM**
electromagnetic-heat-flow	54.2	52.7	57.6	51.3
flow-heat	50.1	47.1	53	46.2

As you can see from Table 4, the maximum temperature difference between unidirectional coupling and bidirectional coupling is 4.6 °C. Therefore, temperature has a great influence on the material properties of the motor electromagnetic field.

Figure 13a is the simulation result considering electromagnetic-heat and flow-heat coupling factors, and Figure 13b shows that the electromagnetic-heat coupling factor is not considered, only the flow-heat coupling factor is considered. By comparing unidirectional and bidirectional coupling, it can be concluded that the maximum temperature difference of IWM is 4.6 °C. It can be seen that, in the case of considering the coupling factor of the motor, the loss and temperature of the motor can be calculated more accurately, ensuring the accuracy of the calculation results.

At the same time, in order to analyze the degree of influence of the flow-heat coupling factor on the motor temperature, the electromagnetic-heat coupling factor is considered, but the flow-heat coupling factor is not considered. The simulation results are shown in Figure 14, and compared with Figure 13a.

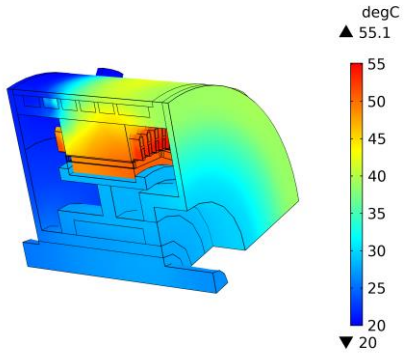

Figure 14. Three-field simulation without considering the fluid-heat coupling factors.

As can be seen from Figure 14 and Table 5, the flow-heat coupling factors also have a great influence on the motor temperature, and the maximum temperature difference is 2.5 °C.

Table 5. Comparison of IWM maximum temperature.

	Maximum Temperature (°C)			
	Stator Core	**Rotor Core**	**Winding**	**PM**
flow-heat coupling factors	54.2	52.7	57.6	51.3
without fluid-heat coupling factors	52.1	50.7	55.1	50.2

5.2. Vehicle Working Condition Setting

When a car is driving in a city, it needs frequent vehicle acceleration, deceleration and so on. Therefore, this paper designed a cycle condition; it includes acceleration, deceleration, uniform speed in rated working condition and high-power driving in peak working conditions. The working condition diagram is shown in Figure 15.

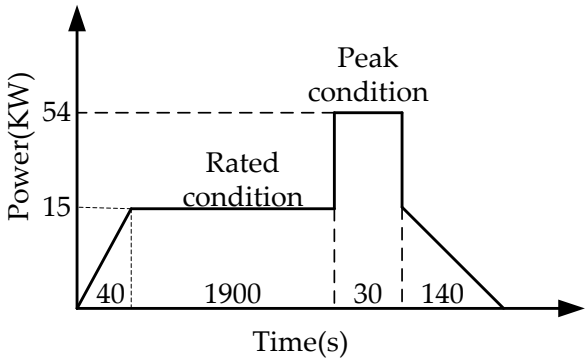

Figure 15. Schematic diagram of cycle conditions.

As shown in Figure 15, the rated working condition is 1000 r/min, the power is 15 KW, the peak working condition is 1100 r/min, and the power is 54 KW. Notably, 0–40 s is the acceleration condition, 40–1940 s is driven at a uniform speed under a rated condition, 1940–1970 s is driving at peak condition, and 1970–2110 s is the deceleration condition.

5.3. Analysis of Electromagnetic Field Simulation Results of IWM

In this paper, COMSOL multiphysics finite element simulation software is used to realize the simulation analysis of four cycle conditions; the total running time is 8440 s. The flux density, loss of each component and electromagnetic torque of the motor are shown in Figure 16. In order to

display the calculated results more clearly, the torque graph has been partially amplified in this paper, and other data graphs will not be repeated.

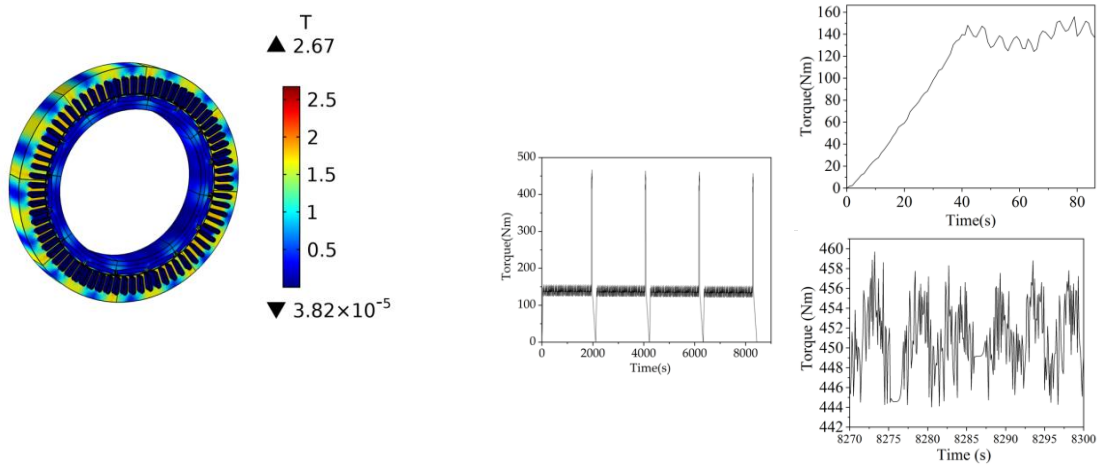

(**a**) Flux density (**b**) Torque

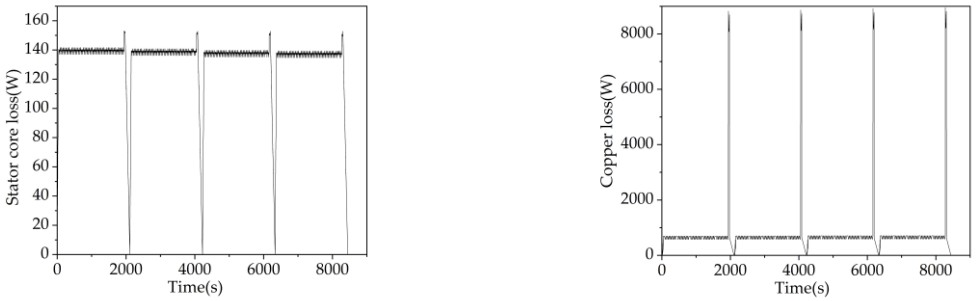

(**c**) Stator core loss (**d**) Copper loss

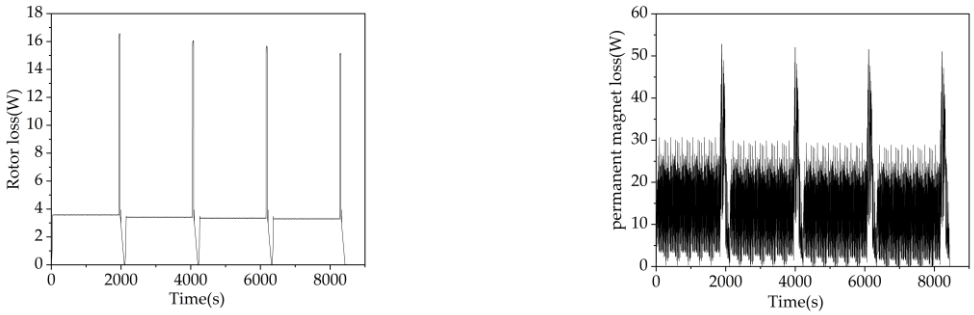

(**e**) Rotor core loss (**f**) Eddy current loss of PM

Figure 16. Time-varying curve of electromagnetic torque and the loss of motor.

As can be seen from Figure 16, after the IWM runs 8440s, among them, the stable part is the simulation result of the rated condition, while the sharply changing part is the simulation result of peak condition. Under rated working condition, the loss of stator core is reduced from 137.36 W to 135.6 W, the loss of rotor core decreases from 3.57 W to 3.29 W, the loss of PM loss decreases from 14.9 W to 13.1 W, the loss of copper loss increases from 645.36 W to 664.89 W, and the torque decreases from 138.6 Nm to 134.2 Nm. Under peak working condition, the loss of stator core decreases from 150.26 W to 147.29 W, the loss of rotor core decreases from 16.41 W to 15.07 W, the loss of PM loss

decreases from 35.96 W to 32.67 W, the loss of copper loss increases from 8330W to 8460.4 W, and the torque decreases from 460.81 Nm to 451.36 Nm.

5.4. Analysis of Temperature Field Simulation Results of IWM

When the IWM, with spiral cooling structure, runs under cyclic conditions, the temperature diagram and temperature change curve of each component within the motor are shown in Figure 17.

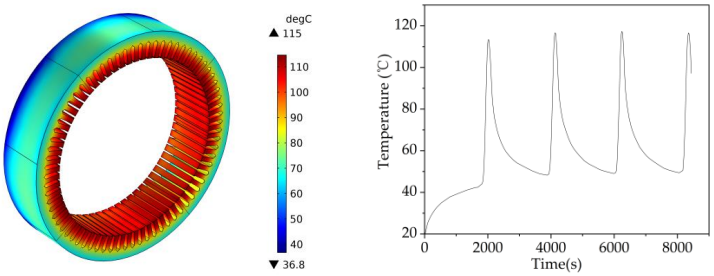

(**a**) Stator core temperature and temperature variation curve.

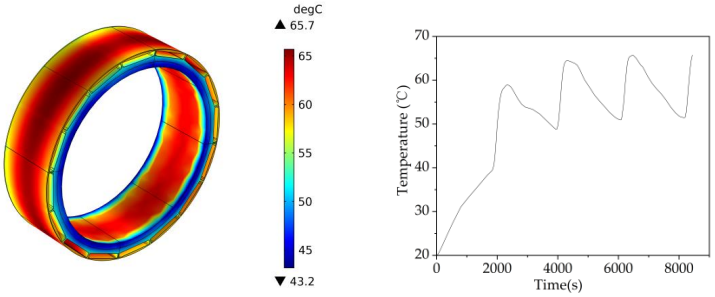

(**b**) Rotor core temperature and temperature variation curve.

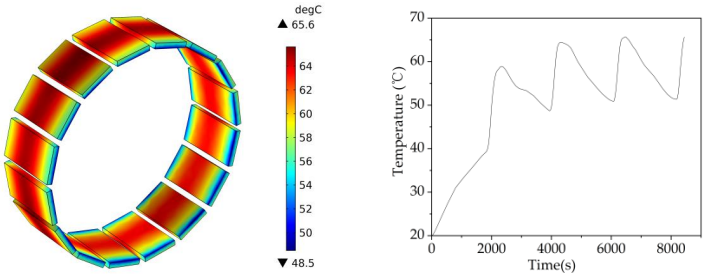

(**c**) PM temperature and temperature variation curve.

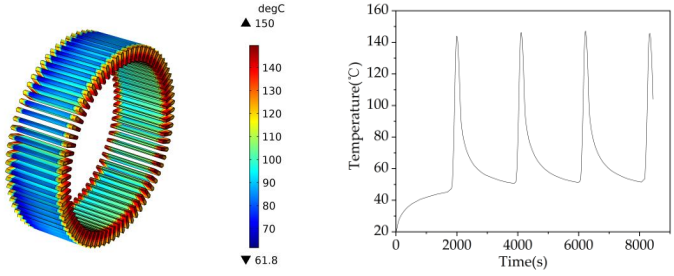

(**d**) Stator winding temperature and temperature variation curve.

Figure 17. Temperature of each component of IWM.

It can be seen from Figure 17a that the stator core temperature of the motor is higher, second only to the stator winding; it is because the stator winding generates a lot of heat during the running of the

motor, and it is transmitted to the stator core by heat conduction. Moreover, the stator core itself also produces loss, which makes the temperature higher; it can also be seen that the temperature of the stator yoke is lower than that of the stator tooth. The main reason is that the stator yoke is close to the housing and cooling channel, and the stator tooth is close to the winding, so that the temperature difference between the yoke and the tooth is large. As can be seen from Figure 17b,c, the temperature of the rotor core is relatively low and substantially equal to the temperature of the PM; the main reason is that there is an air gap between the stator core and the rotor core, and the thermal conductivity of the air gap is low, and the heat conduction is poor, and the loss of rotor core is relatively low, therefore, the overall temperature of the rotor core is lower than that of the stator core, the PM is embedded in the rotor core, and its loss is relatively low, and the PM conducts heat between the rotor core, so that the highest temperature of the two is equal. As can be seen from Figure 17d, the temperature of the insulation layer and the stator winding near the side of the stator core is relatively low, while the temperature of the insulation layer and the stator winding near the side of the air gap is relatively high, because of the contact with the stator core, and heat is transferred through heat conduction, and the thermal conductivity of the silicon steel sheet is much larger than the air gap, so that the insulation layer and the stator winding near the air gap side have poor heat dissipation and a high temperature.

5.5. Analysis of Flow Field Simulation Results of IWM

The cooling structure of IWM is a spiral structure, and after running in cyclic conditions, the velocity of cooling water and velocity curve of cooling water are shown in Figure 18.

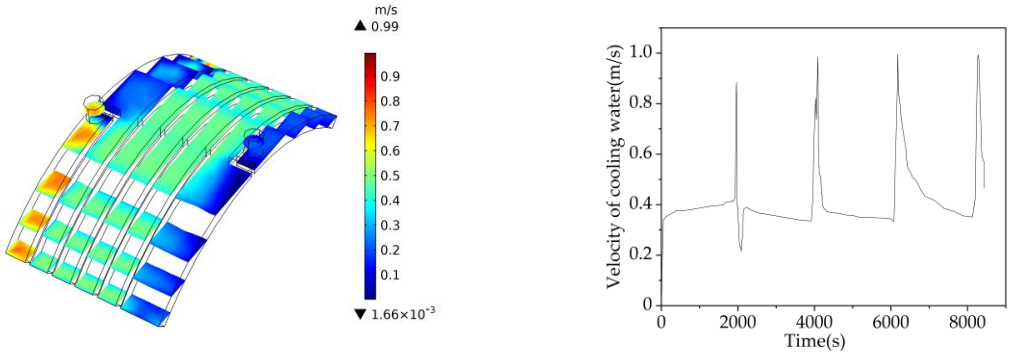

(**a**) Velocity of cooling water (**b**) Velocity curve of cooling water

Figure 18. Cooling water velocity and velocity variation curve of IWM.

As shown in Figure 18a, the highest velocity is 0.99 m/s on the inlet side, and the lowest velocity is close to zero on the outlet side; the velocity in the middle part is approximately 0.3–0.6 m/s. As shown in Figure 18b, as the temperature increases, so does the flow rate, because the dynamic viscosity and density of water decrease with the increase of temperature.

5.6. Variation of Maximum Temperature of IWM at Different Flow Rates

The flow rate of IWM is 0.11 m/s under rated conditions and the flow rate of IWM is 0.76 m/s under peak conditions; the velocity step is 0.04 m/s. Based on the simulation analysis of IWM under different flow velocities, the maximum temperature variation curve of IWM is obtained, as shown in Figure 19.

As can be seen from Figure 19, the flow rate in rated conditions increased from 0.11 m/s to 0.31 m/s, and the flow rate in peak conditions increased from 0.76 m/s to 0.96 m/s; the maximum temperature of IWM was reduced from 150 °C to 146.3 °C, with a total decrease of 3.7 °C. It can be seen that the maximum temperature of the hub motor decreases gradually with the decrease of the flow velocity in a certain range.

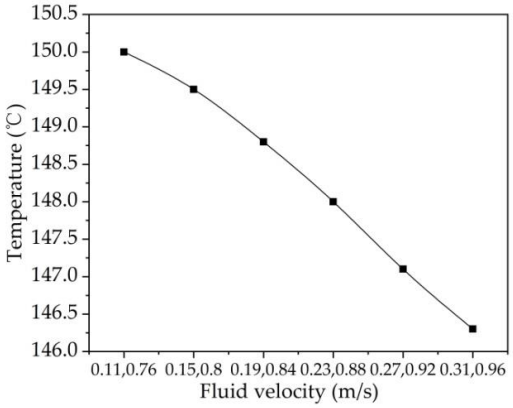

Figure 19. Curve of maximum temperature of IWM with flow velocity.

6. Results

According to the driving conditions of the vehicle, the coupling simulation analysis of electromagnetic field, temperature field and flow field was carried out. The following conclusions are drawn:

(1) There are coupling factors between electromagnetic field, temperature field and flow field, including strong coupling factors and weak coupling factors. The strong coupling factors are electromagnetic-heat coupling factors and flow-heat coupling factors, while the weak coupling factors are electromagnetic-flow coupling factors. The influence factors of the electromagnetic field and temperature field are mainly reflected in the effect of temperature on the conductivity of the motor components and the residual flux density of the PM. The influence factors of temperature field and flow field are mainly reflected in the effect of temperature on the thermal conductivity, specific heat capacity, dynamic viscosity and density of cooling water. The influence factors of the electromagnetic field and flow field are mainly reflected in the effect of alternating electromagnetic fields generated by the electromagnetic field on fluid properties and the effect of flow field on the electromagnetic flux density of IWM.

(2) In the three-field coupling simulation based on the rated working conditions, considering the electromagnetic-thermal coupling factors, the maximum temperature of IWM is increased by 4.6 °C, and compared with that of the unidirectional coupling. Considering the flow-heat coupling factors, the maximum temperature of IWM is reduced by 2.5 °C, and compared with that of unidirectional coupling. It is fully stated that the coupling between multiple fields must be taken into account in calculating the loss and temperature of IWM; this can ensure the accurate calculation of components loss and the temperature of the motor, and also provide a certain reference value for future motor design.

(3) Using the three-field coupling analysis model built in this paper, under cyclic conditions, the characteristics of the electromagnetic field, temperature field and flow field of IWM are analyzed; the results show that the highest temperature of the motor is 150 °C, which does not exceed the insulation grade requirements of the motor (155 °C), the highest temperature of the PM is 65.6 °C, which does not exceed the highest operating temperature of the PM (150 °C).

Although the highest temperature of the IWM does not exceed the insulation grade of the motor, its value is very close, so the next step needs to further optimize the structure of the IWM.

Author Contributions: Conceptualization, D.T.; Data curation, H.X. and C.Z.; Methodology, H.X.; Project administration, D.T.; Software, H.X.; Supervision, D.T.; Validation, S.L. and M.Y.; Writing—original draft, H.X.; Writing—review & editing, S.L., M.Y. and C.Z. All authors have read and agreed to the published version of the manuscript.

Funding: This research was funded by the National Natural Science Foundation of China (grant number 51775320 and 51605265), and sponsored by the Key Technology Research and Development Program of Shandong (grant number 2019GGX104069).

Conflicts of Interest: The authors declare no conflict of interest.

References

1. Shanlin, J. High-Speed Permanent Magnet Synchronous Motor Loss Analysis and Temperature Field Calculation. Ph.D. Thesis, Harbin Institute of Technology, Harbin, China, 2010.
2. Driesen, J.; Paner, U.; Belmans, R.; Hameyer, K. Transient coupled magnetic thermal analysis of a permanent magnet synchronous electrical vehicle motor. In Proceedings of the International Conference on Electrical Machines (ICEM 2000), Espoo, Finland, 28–30 August 2000; pp. 343–347.
3. Alberti, L.; Bianchi, N. A Coupled Thermal-Electromagnetic Analysis for a Rapid and Accurate Prediction of IM Performance. *IEEE Trans. Ind. Electron.* **2008**, *55*, 3575–3582. [CrossRef]
4. Mezani, S.; Takorabet, N.; Laporte, B. A Combined Electromagnetic and Thermal Analysis of Induction Motors. *IEEE Trans. Magnet.* **2005**, *41*, 1572–1575. [CrossRef]
5. Zhang, Q.; Wang, W.; Huang, S.; Guo, J. Heat transfer simulation of high density permanent magnet motor for vehicles based on fluid-solid coupling method. *Electr. Mach. Control Appl.* **2012**, *8*, 1–5.
6. Wang, X.; Jia, Z.; Gao, P. Coupled electromagnetic-thermal field analysis of out-rotor in-wheel motor. *J. Tianjin Univ. Sci. Technol.* **2014**, *47*, 898–902.
7. Hatziathanassiou, V.; Xypteras, J.; Archontoulakis, G. Electrical-thermal coupled calculation of an asynchronous machine. *Archiv ffir Elektrotechnik* **1994**, *77*, 117–122. [CrossRef]
8. Zhao, N.; Liu, W. Electromagnetic Field and Thermal Field Coupling Analysis of Brushless DC Motor. *Small Spec. Electr. Mach.* **2009**, *3*, 9–11.
9. Gao, N.; Yu, L. Research on loss and electromagnetic heat coupling of high speed permanent magnet synchronous moor. In Proceedings of the 2013 IEEE International Conference on Mechatronics and Automation, Takamatsu, Japan, 4–7 August 2013.
10. Zhang, M.; Weiguo, L. Transient Coupled Electro-magnetic Thermal Analysis of a Permanent Magnet Brushless DC Motor. In Proceedings of the 2010 International Conference on Computer, Mechatronics, Control and Electronic Engineering, Changchun, China, 24–26 August 2010.
11. Xiaowei, W.; Tiecai, L. A 3-D Electromagnetic Thermal Coupled Analysis of Permanent Magnet Brushless. In Proceedings of the 2011 First International Conference on Instrumentation, Measurement, Computer, Communication and Control, Beijing, China, 21–23 October 2012.
12. Zhang, L.; Li, C.; Wu, Y.; Zhang, K.; Shi, H. Hybrid Prediction Model of the Temperature Field of a Motorized Spindle. *Appl. Sci.* **2017**, *7*, 1091. [CrossRef]
13. Park, J.B.; Moosavi, M.; Toliyat, H.A. Electromagnetic-Thermal Coupled Analysis Method for Interior PMSM. In Proceedings of the 2015 IEEE International Electric Machines & Drives Conference (IEMDC), Coeur d'Alene, ID, USA, 10–13 May 2015; pp. 1209–1214.
14. Karnavas, Y.L.; Chasiotis, I.D.; Peponakis, E.L. Cooling System Design and Thermal Analysis of an Electric Vehicle's In-Wheel PMSM. In Proceedings of the 2016 XXII International Conference on Electrical Machines (ICEM), Lausanne, Switzerland, 4–7 September 2016; pp. 1439–1445.
15. Lamghari-Jamal, M.I.; Fouladgar, J.; Zaim, E.H.; Trichet, D. A Magneto-Thermal Study of a High-Speed Synchronous Reluctance Machine. *IEEE Trans. Magn.* **2006**, *42*, 1271–1274. [CrossRef]
16. Li, J.Q.; Ma, S.L.; Li, H.M. Analysis and calculation on stator temperature field of turbo-generators based on couple physical field. *J. North China Electric Power Univ.* **2008**, *35*, 6–10.
17. Ding, S.Y.; Ge, Y.Z.; Chen, W.J.; Xu, D.G.; Miao, L.J. Coupling calculation and analysis of Three-dimensional temperature field for doubly-fed wind generator. *Electric Mach. Control* **2012**, *16*, 83–88.
18. Song, F. Research on Heating and Cooling System of Hub Motor Drive System. Master's Thesis, Shandong University of Technology, Harbin, China, 2019.
19. Yin, H. PMSM Loss Calculation and Temperature Field Analysis. Master's Thesis, Harbin Institute of Technology, Harbin, China, 2015.
20. Bertotti, G.; Boglietti, A.; Chiampi, M.; Chiarabaglio, D.; Fiorillo, F.; Lazzari, M. An Improved Estimation of Iron Losses in Rotating Electrical Machines. *IEEE Trans. Magn.* **1991**, *27*, 5007–5009. [CrossRef]
21. Ping, C.; Renyuan, T.; Wenming, T.; Jianguo, J.; Qingliang, D. Permanent magnet eddy current loss and its influence of high power density permanent magnet synchronous motor. *Trans. China Electrotech. Soc.* **2015**, *30*, 1–9.

22. Lim, D.H.; Kim, S.C. Thermal performance of oil spray cooling system for in-wheel motor in electric vehicles. *Appl. Therm. Eng.* **2014**, *63*, 577–587. [CrossRef]
23. Chen, W. Desigh and Temperature Analysis of Permanent Magnet Synchronous Motor for Electric Vehicles. Master's Thesis, Harbin Institute of Technology, Harbin, China, 2013.
24. Tang, R. *Modern Permanent Magnet Machines*; China Machine Press: Beijing, China, 2015.
25. Yang, S.; Tao, W. *Heat Transfer*; Higher Education Press: Beijing, China, 2006.
26. Liu, Q.S.; Yan, P.F.; Yang, M.; Tan, Z.C.; Li, C.P.; Welz-Biermann, U. Dynamic viscosity and conductivity of ionic liquids. *Acta Phys. Chim. Sin.* **2011**, *27*, 2762–2766.
27. Sun, J.X.; Sun, Y.X.; Wang, Y.B. Two—Dimensional steady temperature field analysis of interior permanent magnet synchronous motor. *Small Special Electr. Mach.* **2013**, *41*, 24–33.
28. Pechánek, R.; Bouzek, L. Analyzing of Two Types Water Cooling ElectricMotors Using Computational Fluid Dynamics. In Proceedings of the 15th International Power Electronics and Motion Control Conference, Novi Sad, Serbia, 4–6 September 2012; pp. LS2e4-1–LS2e4-5.
29. Wang, R.-J.; Heyns, G.C. Thermal Analysis of a Water-Cooled Interior Permanent Magnet Traction Machine. In Proceedings of the 2013 IEEE International Conference on Industrial Technology (ICIT), Cape Town, South Africa, 25–28 Febuary 2013; pp. 416–421.